Communications in Nonlinear Science and Numerical Simulation 126 (2023) 107461

Contents lists available at ScienceDirect

Communications in Nonlinear Science and Numerical Simulation

journal homepage: www.elsevier.com/locate/cnsns

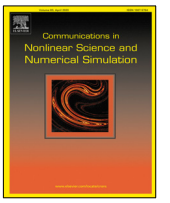

Research paper

The impact of heterogeneous human activity on vegetation patterns in arid environments

Li-Feng Hou [a,b], Gui-Quan Sun [a,b,*], Matjaž Perc [c,d,e,f,g]

[a] Department of Mathematics, North University of China, Taiyuan 030051, Shanxi, China
[b] Complex Systems Research Center, Shanxi University, Taiyuan 030006, Shanxi, China
[c] Faculty of Natural Sciences and Mathematics, University of Maribor, Koroška cesta 160, 2000 Maribor, Slovenia
[d] Department of Medical Research, China Medical University Hospital, China Medical University, Taichung 404332, Taiwan
[e] Alma Mater Europaea, Slovenska ulica 17, 2000 Maribor, Slovenia
[f] Complexity Science Hub Vienna, Josefstädterstraße 39, 1080 Vienna, Austria
[g] Department of Physics, Kyung Hee University, 26 Kyungheedae-ro, Dongdaemun-gu, Seoul, Republic of Korea

ARTICLE INFO

Article history:
Received 9 October 2022
Received in revised form 16 July 2023
Accepted 22 July 2023
Available online 26 July 2023

Keywords:
Human activities
Spatial heterogeneity
Vegetation patterns
Optimal control

ABSTRACT

Vegetation patterns have attracted increasing interest in recent years since they can be used as a key indicator of ecosystem robustness. As one of the vital factors affecting vegetation structures, human activities have been widely explored in the literature. Nevertheless, the effects of spatiotemporal heterogeneity of human activities on vegetation patterns are far from being well explained. Here, we address this issue by applying optimal control theory to the dryland vegetation-water model. We find that the spatiotemporal heterogeneity of human activities leads to the transition from different states to desired vegetation patterns, including the spot, labyrinth, and gap patterns, and thus increases the diversity of pattern structures. The heterogeneity in human activities is also found to promote the vegetation growth in low-rainfall areas, which in turn effectively prevents vegetation desertification. Our robustness analysis fully supports these findings. This work well quantitatively links human activities with ecosystems robustness and helps provide new insights for biodiversity conservation.

© 2023 Elsevier B.V. All rights reserved.

1. Introduction

The natural environment's vegetation, an assemblage of various plant species and their ground cover, is essential to maintaining ecosystem health. For instance, vegetation can slow down the greenhouse by reducing air pollution [1,2], as well as help arid areas conserve water and soil resources via reducing soil erosion. In addition to these direct impacts on ecosystems, vegetation is also capable of serving as an indicator of ecosystems degradation, which has attracted growing interest [3,4].

Vegetation usually displays even but regular spatial distributions, which are known as vegetation patterns. Vegetation patterns have been observed all over the world so far in a wide variety of forms [5–7]. Such patterns are primarily formulated through the interactions between vegetation and water resources [8,9]. To further investigate the mechanism behind such patterns, numerous dynamical models have been proposed, which are broadly categorized into univariate [10–12], bivariate [6,13–15], and three-variable models [5,7,16] according to the number of variables taken into account. In

* Corresponding author at: Department of Mathematics, North University of China, Taiyuan 030051, Shanxi, China.
E-mail addresses: sunguiquan@sxu.edu.cn (G.-Q. Sun), matjaz.perc@gmail.com (M. Perc).

https://doi.org/10.1016/j.cnsns.2023.107461
1007-5704/© 2023 Elsevier B.V. All rights reserved.

general, the number of variables depends on whether or not the water dynamics and types of water are considered. Accounting only for vegetation evolution, for example, Lefever and Lejeune established a univariate model to describe the dynamics of terrestrial plant communities in arid areas [10]. Taking the water dynamics into account, Klausmeier proposed a bivariate model, i.e., a vegetation-water model, and found that each component of the model is essential for the formation of vegetation patterns [6]. Moreover, three-variable models can be developed by considering water types, such as surface water and soil water [17], and are capable of characterizing complex interactions in the system as well as revealing the critical role vegetation plays in maintaining the ecosystem's health [5]. Along with the growing literature on investigating vegetation formation [18–22], the mystery of complex mechanisms behind the vegetation patterns and their comprehensive functions is being uncovered.

It has always been a research hotspot to explore the related factors affecting the formation of vegetation patterns [20,21,23], which are mainly divided into two categories: natural factors (such as temperature, rainfall, light, CO_2, etc.) and human activities (such as grazing, felling, afforestation, etc.). Among them, human activities have three typical characteristics, namely purpose, dependence and knowledge, and are subject to the constraints of various policies and regulations. In other words, the impact of human activities on vegetation in arid and semi-arid areas is controllable. Hence, it is more practical to study the influence of human activities on vegetation patterns. At present, there are some studies on this [24–27]. For example, Ge et al. established a vegetation-animal model based on the principle of phase separation to study the effect of grazing on the formation of vegetation patterns [26]. Cao et al. illustrated that afforestation is an effective means to prevent desertification and soil erosion, but improper afforestation will exacerbate environmental degradation in ecologically fragile area [25]. We can see that most of these studies are based on single human activities, that is, only grazing or only afforestation. Obviously, these elements can be classified as human activities. Therefore, this paper comprehensively considers a variety of human factors and takes human activities as an overall influencing factor to study their impact on vegetation pattern structures.

Spatial heterogeneity refers to the heterogeneity and complexity of the spatial distribution of ecological processes and patterns. It has attracted attention and application in various fields [28,29], especially in the field of ecology. For example, Gandhi et al. studied the impact of terrain heterogeneity on the formation of vegetation patterns [30]. Bastiaansen et al. used spatial heterogeneity to study fragmented tipping [31]. However, there are few studies on the effect of spatial heterogeneity of human activities on vegetation patterns. Obviously, due to the subjectivity of human activities, it is necessary to consider the impact of such spatio-temporal heterogeneity on vegetation. Based on this, this paper combined optimal control methods to reveal the impact of the spatial heterogeneity of human activities on the vegetation pattern.

Optimal control theory is a subject that studies and solves to find the optimal solution from all possible control schemes. Currently, it has been successfully utilized to identify the most effective measures for disease prevention and control [32–34] as well as to study the impact of network topological changes on network patterns [35,36]. However, this method is rarely applied in ecology. This paper will unravel the impacts of spatiotemporal heterogeneity of human activities and link the heterogeneity to explicit pattern structures for different parameter conditions under the theoretical framework of the combination of optimal control and dryland vegetation model, so as to provide fresh perspectives on further understanding the interaction between human activities, ecosystem robustness, and biodiversity.

The rest of the paper is organized as follows. Section 2 provides the detail of the model and related analysis, of which the objective functional and its corresponding optimal control problem are given in Section 2.3. The numerical results shown in Section 3 then demonstrates how vegetation patterns are influenced by human activities with and without spatial heterogeneity. Section 4 finally comes to the conclusion and discussion.

2. Mathematical model and analysis

2.1. Model formulation

In an arid environment, water plays an important role in the growth of vegetation, which in turn affects the water dynamics. Some existing models have taken into account this fact. For instance, Gilad et al. developed a three-variable model with multiple interactions between vegetation and water, including osmosis feedback, root-extension feedback, and soil moisture diffusion feedback [5]. Meron et al. proposed a simplified model by incorporating some realistic factors and the root characteristics of some vegetation [19]. Getzin et al. further proved that the spatial self-organization gives rise to the fairy circles based on the simplified model [37]. All these models were based on the assumption that the water layer is thin. However, in some areas of an arid environment, the water layer is actually very thick [38]. Besides, the impact of human activities on vegetation patterns has not been considered in these models. In view of these issues, in this paper we integrate human activities into the extended version of the model by Gilad et al. [5] and propose the following model:

$$\begin{cases} \partial_t b = g_b b(1-b) - b + r + \nabla^2 b \triangleq f_1(b,w,h,r) + \nabla^2 b, & in\ Q = \Omega \times (0,T) \\ \partial_t w = Ih - l_w w - g_w w + \delta_w \nabla^2 w \triangleq f_2(b,w,h,r) + \delta_w \nabla^2 w, & in\ Q \\ \partial_t h = p - Ih - l_h h + \delta_h \nabla^2 h \triangleq f_3(b,w,h,r) + \delta_h \nabla^2 h, & in\ Q \end{cases} \tag{1}$$

where

$$I = \alpha\frac{b+qf}{b+q}, \quad l_w = \frac{\nu_w}{1+R_w b}, \quad l_h = \frac{\nu_h}{1+R_h b},$$

and

$$g_b = w(1+\eta b)^2, \quad g_w = \gamma b(1+\eta b)^2.$$

In system (1), $b(x,t)$ stands for the biomass of plants, $w(x,t)$ represents the water within soil, and $h(x,t)$ is the surface water. In the first equation, the $g_b b(1-b)$ term refers to vegetation growth driven by water absorption of vegetation, the b term corresponds to the natural death of vegetation, and the r term is due to the effect of human activities on vegetation, which can be either positive or negative. If $r > 0$, it corresponds to human activities that promote vegetation growth, such as planting and forestation. If $r < 0$, it represents human activities that are detrimental to vegetation growth, such as logging and grazing. In the second equation, the Ih term represents water that seeps into the soil, the terms $l_w w$ and $g_w w$ represent the loss of soil moisture caused by evaporation and water absorption of vegetation, respectively. In the third equation, the p term represents the gain of surface water due to rainfall and the $l_h h$ term stands for the loss of surface water due to evaporation. Ω represents the spatial domain. Note that zero-flux boundary conditions are chosen in our model and the specific meaning of each parameter and the corresponding dimensionless transformation can be found in Refs. [5,19].

2.2. Conditions for vegetation patterns in system (1) with homogeneous environments

In order for a comparison between the system with homogeneous human activities and the system with heterogeneous human activities, we first consider the simplest case where the human activities are spatially homogeneous and do not change over time. Therefore, in this case we assume the human activities parameter r is constant. In what follows, we present a analysis for the dimensionless model (1). It is easy to obtain the equilibrium point $E^*(b^*, w^*, h^*)$ of system (1) as follows:

$$w^* = \frac{-r+b^*}{b^*(1+\eta b^*)^2(1-b^*)}, \quad h^* = \frac{p}{J+l_h},$$

where b^* is the solution of a unary seventh-degree equation, which is hard to derive analytically. In order to ensure the positivity of the equilibrium point $E^*(b^*, w^*, h^*)$, the following conditions need to be met

$$\begin{cases} r < b^* < 1, & if\ 0 < r < 1, \\ 1 < b^* < r, & if\ r > 1, \\ 0 < b^* < 1, & if\ r < 0. \end{cases}$$

Furthermore, by assuming $b_x^t = b^* + \alpha_1 \exp(\lambda t)\exp(ik\bullet x)$, $w_x^t = w^* + \alpha_2 \exp(\lambda t)\exp(ik\bullet x)$, and $h_x^t = h^* + \alpha_3 \exp(\lambda t)\exp(ik\bullet x)$, and linearizing the system (1) at the equilibrium point $E^*(b^*, w^*, h^*)$, we can get the Jacobian matrix as

$$J_k = \begin{pmatrix} a_{11}-k^2 & a_{12} & 0 \\ a_{21} & a_{22}-\delta_w k^2 & a_{23} \\ a_{31} & 0 & a_{33}-\delta_h k^2 \end{pmatrix},$$

where the expression of $a_{ij}(i = 1, 2, 3; j = 1, 2, 3)$ can be found in Appendix. Denote λ_k as the corresponding eigenvalue of J_k.

By solving the characteristic equation of the above matrix, we can get the following dispersion relation:

$$\lambda^3 + c_1(k)\lambda^2 + c_2(k)\lambda + c_3(k) = 0,$$

where

$$\begin{aligned} c_1(k) =& (\delta_w + \delta_h + 1)k^2 - a_{11} - a_{22} - a_{33}, \\ c_2(k) =& (\delta_h\delta_w + \delta_h + \delta_w)k^4 - (a_{11}\delta_h + a_{11}\delta_w + a_{22}\delta_h + a_{33}\delta_w + a_{22} + a_{33})k^2 + a_{11}a_{22} + \\ & a_{11}a_{33} - a_{12}a_{21} + a_{22}a_{33}, \\ c_3(k) =& \delta_h\delta_w k^6 - (a_{11}\delta_h\delta_w + a_{22}\delta_h + a_{33}\delta_w)k^4 + (a_{11}a_{22}\delta_h + a_{11}a_{33}\delta_w - a_{12}a_{21}\delta_h + a_{22}a_{33})k^2 \\ & - a_{11}a_{22}a_{33} + a_{12}a_{21}a_{33} - a_{12}a_{23}a_{31}. \end{aligned}$$

For a spatially uniform disturbance (i.e. $k = 0$), if the equilibrium point $E^*(b^*, w^*, h^*)$ satisfies the following conditions:

$$\begin{cases} c_1(0) = -a_{11} - a_{22} - a_{33} > 0, \\ c_3(0) = -a_{11}a_{22}a_{33} + a_{12}a_{21}a_{33} - a_{12}a_{23}a_{31} > 0, \\ c_1(0)c_2(0) - c_3(0) > 0, \end{cases}$$

then the Routh–Hurwitz criterion can guarantee that all eigenvalues have negative real parts, thus making the equilibrium point $E^*(b^*, w^*, h^*)$ stable. Similarly, for a spatially inhomogeneous perturbation (i.e. $k \neq 0$), if any of the aforementioned conditions are not satisfied, it indicates that the characteristic equation has positive real part eigenvalues, so that the equilibrium point $E^*(b^*, w^*, h^*)$ is unstable and Turing branches occur. Obviously, $c_1(k) > 0$ since $c_1(0) > 0$ and δ_w, δ_h, $k > 0$. Therefore, we only need to determine the sign of $c_3(k)$ and $c_1(k)c_2(k) - c_3(k)$. Below, we will analyze them separately,

Case 1. Analyze the sign of $c_3(k)$.

Let $c_3(k) = d_3(k^2)$ and $e = k^2$, we get

$$d_3(e) = g_3e^3 + g_2e^2 + g_1e + g_0,$$

where $g_3 = \delta_h\delta_w$, $g_2 = a_{11}\delta_h\delta_w + a_{22}\delta_h + a_{33}\delta_w$, $g_1 = a_{11}a_{22}\delta_h + a_{11}a_{33}\delta_w - a_{12}a_{21}\delta_h + a_{22}a_{33}$ and $g_0 = -a_{11}a_{22}a_{33} + a_{12}a_{21}a_{33} - a_{12}a_{23}a_{31}$. The following analysis is performed on the polynomial $d_3(e)$:

(i) $\lim_{e\to+\infty} d_3(e) = +\infty$.

(ii) Calculate the first and second order partial derivatives of $d_3(e)$.

$$\frac{\mathrm{d}d_3(e)}{\mathrm{d}e} = 3g_3e^2 + 2g_2e + g_1, \quad \frac{\mathrm{d}^2d_3(e)}{\mathrm{d}e^2} = 6g_3e + 2g_2.$$

The two extreme points of $d_3(e)$ can be obtained by simple calculation as

$$e_{1,2} = \frac{-g_2 \pm \sqrt{g_2^2 - 3g_3g_1}}{3g_3} \quad with\ g_2^2 - 3g_3g_1 > 0.$$

Since $g_3 > 0$, $d_3(e)$ is a concave function with an upward opening as $e \to \infty$. Also, we can obtain the relationship between the two extremal points according to the properties of the cubic function

$$e_{\max} = e_2 < e_1 = e_{\min}.$$

(iii) if $e_1 > 0$ and $d_3(e_{\min}) = d_3(e_1) < 0$, then Turing instability occurs.

In summary, the conditions for Turing instability to occur are

$$\begin{cases} c_1(0) > 0,\ c_3(0) > 0,\ c_1(0)c_2(0) - c_3(0) > 0, \\ g_2^2 - 3g_3g_1 > 0,\ e_1 > 0,\ d_3(e_{\min}) = d_3(e_1) < 0. \end{cases}$$

Case 2. Analyze the symbols of $c_1(k)c_2(k) - c_3(k)$.

The analysis process of $c_1(k)c_2(k) - c_3(k)$ is similar to that of $c_3(k)$, so we will not elaborate further.

The difficulty of obtaining an analytical solution for the equilibrium point and the complexity of the model itself lead to the fact that in linear stability analysis we can only give an approximate analytical framework and cannot give a detailed range of values for each parameter. Therefore, we resort to the numerical solution by using the parameter values given in Table 1. In the case of $r > 0$, which means that human activities facilitate vegetation growth, we set $r = 0.0002$ and then the system (1) has the following three equilibrium points:

$$E_0^*(b_0^*, w_0^*, h_0^*) = (0.0005, 0.6006, 0.7328);$$

$$E_1^*(b_1^*, w_1^*, h_1^*) = (0.0277, 0.9668, 0.5674);$$

$$E_2^*(b_2^*, w_2^*, h_2^*) = (0.1646, 0.8817, 0.2777).$$

Moreover, it is easy to obtain that if $r \to 0$ then $b_0^* \to 0$, which corresponds to the desert state. In the case of $r < 0$, which means that human activities impede vegetation growth, we choose $r = -0.0002$ and then the system (1) has the following two equilibrium points:

$$E_1^{*'}(b_1^*, w_1^*, h_1^*) = (0.0295, 0.9789, 0.5595);$$

$$E_2^{*'}(b_2^*, w_2^*, h_2^*) = (0.1636, 0.8843, 0.2787).$$

Direct calculations indicate that the constant solution E_0^* is asymptotically stable in all circumstances. Thus, we hereafter mainly focus on the stability analysis of the equilibrium points E_1^* ($E_1^{*'}$) and E_2^* ($E_2^{*'}$).

It is easy to show that E_2^* (or $E_2^{*'}$) is stable under some suitable conditions. In this case, stationary patterns (Turing patterns) will emerge if $\max \Re(\lambda_k) > 0$, for some $k > 0$ (see Fig. 1(a)). We can also show that E_1^* (or $E_1^{*'}$) is always unstable and thus one can conclude from Ref. [39] that transient patterns can emerge if $0 < \max \Re(\lambda_0) < \max \Re(\lambda_k)$ (see Fig. 1(b)).

Table 1
Values of related parameters in model (1) [37].

p	η	α	γ	q	ν_w
2.1	0.999	60	4.662	1.8018	0.75
ν_h	R_w	R_h	f	δ_w	δ_h
2.25	0.3	0.8	0.01	820	25

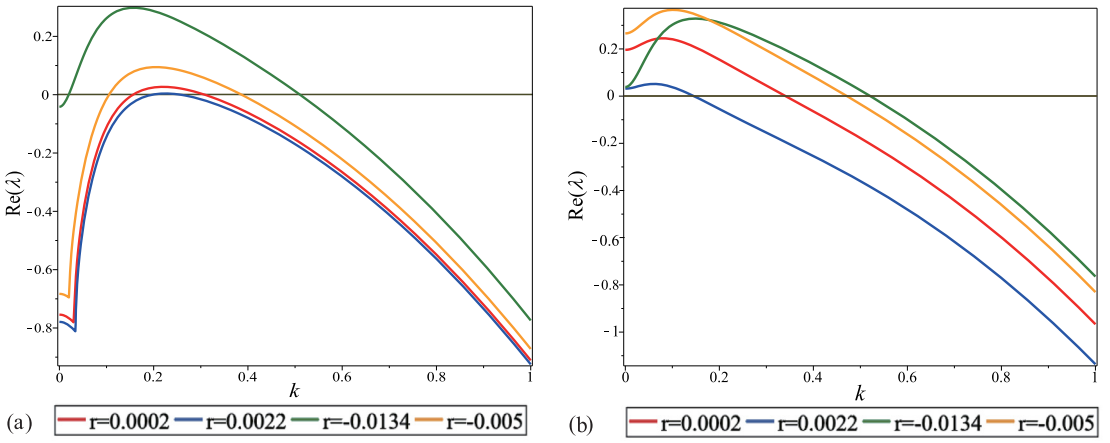

Fig. 1. Dispersion diagram at equilibrium points E_2^* ($E_2^{*'}$) and E_1^* ($E_1^{*'}$) for different intensities of human activities. Panel (a) corresponds to the case where stationary patterns (Turing patterns) appear whereas panel (b) corresponds to the case where transient patterns can emerge. Relevant parameter values are given in Table 1.

2.3. System (1) with spatial heterogeneity: from the viewpoint of optimal control

Now we study system (1) with heterogeneous human activities. In this case, the human activities parameter r is not a constant but rather a variable that depends on both time and space, namely, $r = r_x^t$. We use $r = r_x^t$ as the control parameter. Consider the following optimum control problem[1]

$$\begin{aligned} O_{\min} = \min_{r\in U_{ad}} O[b,w,h,r] =& \frac{a_1}{2}\int_\Omega [b_x^T - b_x^{tar}]^2 dx + \frac{a_2}{2}\int_\Omega [w_x^T - w_x^{tar}]^2 dx \\ &+ \frac{a_3}{2}\int_\Omega [h_x^T - h_x^{tar}]^2 dx + \frac{c}{2}\int_0^T\int_\Omega (r_x^t)^2 dxdt, \end{aligned} \tag{2}$$

subject to

$$\begin{cases} \partial_t b = f_1(b,w,h,r) + \nabla^2 b, & in\ Q \\ \partial_t w = f_2(b,w,h,r) + \delta_w \nabla^2 w, & in\ Q \\ \partial_t h = f_3(b,w,h,r) + \delta_h \nabla^2 h, & in\ Q \\ \partial_n b = 0,\ \delta_w \partial_n w = 0,\ \delta_h \partial_n h = 0, & on\ \partial\Omega \times (0,T) \\ b_x^0 = b^0(x),\ w_x^0 = w^0(x),\ v_x^0 = v^0(x), & in\ \Omega \end{cases} \tag{3}$$

where $O[b,w,h,r]$ is the objective functional, a_1, a_2, a_3 and c are positive constants. Additionally, b_x^t, w_x^t and h_x^t are called state variables. b_x^{tar}, w_x^{tar} and h_x^{tar} are target patterns generated by model (1) under parameter values given in Table 1. The set of admissible controls used to determine the control parameter r_x^t is specified by the following form:

$$U_{ad} = \{r \in L^\infty(Q) : r_1 \le r_x^t \le r_2\ a.e.\ in\ Q\}. \tag{4}$$

Theorem 2.1. *If r^* is a locally optimal solution to the optimal control problem (2)–(3), then there are corresponding states (b^*, w^*, h^*) and adjoint states (u_1, u_2, u_3) such that the state system (3), adjoint system (5) and variational inequality (6) are*

[1] There are two main reasons for including the variables of surface water and soil water in the target function. Firstly, since we consider the interactions between vegetation, soil moisture and ground water in the model, the optimal solution we seek should be related to these three variables. Secondly, it is revealed that human activities have impacts on rainfall, thereby affecting the surface water and soil water [40,41].

established:

$$\begin{cases} -\partial_t u_1 = f_{1,b}u_1 + f_{2,b}u_2 + f_{3,b}u_3 + \nabla^2 u_1, & in\ Q \\ -\partial_t u_2 = f_{1,w}u_1 + f_{2,w}u_2 + f_{3,w}u_3 + \delta_w \nabla^2 u_2, & in\ Q \\ -\partial_t u_3 = f_{1,h}u_1 + f_{2,h}u_2 + f_{3,h}u_3 + \delta_h \nabla^2 u_3, & in\ Q \\ \partial_n u_1 = 0, \delta_w \partial_n u_2 = 0, \delta_h \partial_n u_3 = 0, & on\ \partial\Omega \times (0,T) \\ u_{1_x}^T = a_1[b^{*T}_x - b^{tar}_x], & in\ \Omega \\ u_{2_x}^T = a_2[w^{*T}_x - w^{tar}_x], & in\ \Omega \\ u_{3_x}^T = a_3[h^{*T}_x - h^{tar}_x], & in\ \Omega \end{cases} \tag{5}$$

and

$$\int_\Omega \int_0^T (cr^* + u_1)(r - r^*)dtdx \geq 0, \tag{6}$$

where

$$\begin{aligned} f_{1,b} &= -b^* w^* (1 + b^*\eta)^2 - w^*(1 + b^*\eta)^2(b^* - 1) + 2\eta b^* w(1 + b^*\eta)(1 - b^*) - 1, \\ f_{2,b} &= \alpha h \frac{q - qf}{(b^* + q)^2} + \frac{\nu_w R_w w^*}{(1 + R_w b^*)^2} - \gamma w^*(1 + \eta b^*)^2 - 2\gamma \eta b^* w^*(1 + \eta b^*), \\ f_{3,b} &= \frac{\nu_h R_h h^*}{(1 + R_h b^*)^2} - \alpha h^* \frac{q - qf}{(b^* + q)^2}, \\ f_{1,w} &= b^*(1 + \eta b^*)^2(1 - b^*), \quad f_{2,w} = \frac{-\nu_w}{1 + R_w b^*} - \gamma b^*(1 + \eta b^*)^2, \quad f_{3,w} = 0, \\ f_{1,h} &= 0, \quad f_{2,h} = \alpha \frac{b^* + qf}{b^* + q}, \quad f_{3,h} = -\alpha \frac{b^* + qf}{b^* + q} - \frac{\nu_h}{1 + R_h b^*}. \end{aligned}$$

Proof. The strict proof for the necessary optimality condition can be found in Refs. [42–44]. Here, we formally derive the conclusion of Theorem 2.1 by using the Lagrange multiplier method. The Lagrange function is constructed as follows:

$$\begin{aligned} L[b, w, h, r, u_1, u_2, u_3] &= O[b, w, h, r] + \int_0^T \int_\Omega [\partial_t b + f_1(b, w, h, r) + \nabla^2 b]u_1 dxdt \\ &+ \int_0^T \int_\Omega [\partial_t w + f_2(b, w, h, r) + \delta_w \nabla^2 w]u_2 dxdt + \int_0^T \int_\Omega [\partial_t h + f_3(b, w, h, r) + \delta_h \nabla^2 h]u_3 dxdt \\ &- \int_0^T \int_{\partial\Omega} \partial_n b u_1 dsdt - \int_0^T \int_{\partial\Omega} \delta_w \partial_n w u_2 dsdt - \int_0^T \int_{\partial\Omega} \delta_h \partial_n h u_3 dsdt \\ &= O[b, w, h, r] + \int_0^T \int_\Omega \partial_t u_1 b dxdt + \int_\Omega [b^0_x u_{1_x}^0 - b^T_x u_{1_x}^T]dx \\ &+ \int_0^T \int_\Omega \nabla^2 u_1 b dxdt + \int_0^T \int_\Omega f_1(b, w, h, r)u_1 dxdt - \int_0^T \int_{\partial\Omega} \partial_n u_1 b dsdt \\ &+ \int_0^T \int_\Omega \partial_t u_2 w dxdt + \int_\Omega [w^0_x u_{2_x}^0 - w^T_x u_{2_x}^T]dx \\ &+ \int_0^T \int_\Omega \nabla^2 u_2 w dxdt + \int_0^T \int_\Omega f_2(b, w, h, r)u_2 dxdt - \int_0^T \int_{\partial\Omega} \delta_w \partial_n u_2 w dsdt \\ &+ \int_0^T \int_\Omega \partial_t u_3 h dxdt + \int_\Omega [h^0_x u_{3_x}^0 - h^T_x u_{3_x}^T]dx \\ &+ \int_0^T \int_\Omega \nabla^2 u_3 h dxdt + \int_0^T \int_\Omega f_3(b, w, h, r)u_3 dxdt - \int_0^T \int_{\partial\Omega} \delta_h \partial_n u_3 h dsdt. \end{aligned} \tag{7}$$

Given that (b^*, w^*, h^*, r^*) is the local optimal solution of the optimal control problem (2)–(3), for any smooth and sufficiently small b^t_x with $b^0_x = 0$, the directional derivative of Lagrange functional at $(b^*, w^*, h^*, r^*, u_1, u_2, u_3)$ satisfies:

$$\begin{aligned} 0 = L_b[b^*, w^*, h^*, r^*, u_1, u_2, u_3]b &= a_1 \int_\Omega [b^{*T}_x - b^{tar}_x]b^T_x dx \\ &+ \int_\Omega \int_0^T \partial_t u_1 b dtdx - \int_\Omega b^T_x u_{1_x}^T dx + \int_\Omega \int_0^T \nabla^2 u_1 b dtdx \end{aligned}$$

$$
\begin{aligned}
&- \int_{\partial\Omega}\int_0^T \partial_n u_1 b dt ds + \int_\Omega \int_0^T f_{1,b}(b^*, w^*, h^*, r^*)u_1 dt dx \\
&+ \int_\Omega \int_0^T f_{2,b}(b^*, w^*, h^*, r^*)u_2 dt dx + \int_\Omega \int_0^T f_{3,b}(b^*, w^*, h^*, r^*)u_3 dt dx. \qquad (8)
\end{aligned}
$$

In light of the arbitrariness of b_x^t, the adjoint system of u_1 satisfies:

$$
\begin{cases}
-\dfrac{\partial u_1}{\partial t} = f_{1,b}u_1 + f_{2,b}u_2 + f_{3,b}u_3 + \nabla^2 u_1, & in\ Q \\
\dfrac{\partial u_1}{\partial n} = 0, & on\ \partial\Omega \times (0,T) \\
u_{1_x}^T = a_1[b^{*T}_x - b_x^{tar}], & in\ \Omega
\end{cases} \qquad (9)
$$

where $f_{i,b}$ $(i = 1, 2, 3)$ is the derivative of f_i with respect to b.

Similarly, from $L_w[b^*, w^*, h^*, r^*, u_1, u_2, u_3]w = 0$ and $L_h[b^*, w^*, h^*, r^*, u_1, u_2, u_3]h = 0$, we can get:

$$
\begin{cases}
-\dfrac{\partial u_2}{\partial t} = f_{1,w}u_1 + f_{2,w}u_2 + f_{3,w}u_3 + \delta_w \nabla^2 u_2, & in\ Q \\
\delta_w \dfrac{\partial u_2}{\partial n} = 0, & on\ \partial\Omega \times (0,T) \\
u_{2_x}^T = a_2[w^{*T}_x - w_x^{tar}], & in\ \Omega
\end{cases} \qquad (10)
$$

and

$$
\begin{cases}
-\dfrac{\partial u_3}{\partial t} = f_{1,h}u_1 + f_{2,h}u_2 + f_{3,h}u_3 + \delta_h \nabla^2 u_3, & in\ Q \\
\delta_h \dfrac{\partial u_3}{\partial n} = 0, & on\ \partial\Omega \times (0,T) \\
u_{3_x}^T = a_3[h^{*T}_x - h_x^{tar}], & in\ \Omega
\end{cases} \qquad (11)
$$

where $f_{i,w}$ and $f_{i,h}$ (i = 1, 2, 3) are the derivatives of f_i with respect to w and h, respectively.

Since the admissible control set is a closed convex set, the directional derivative of Lagrange functional along $r - r^*$ at (b^*, w^*, h^*, r^*) satisfies the following formula:

$$
\begin{aligned}
0 \le & L_r[b^*, w^*, h^*, r^*, u_1, u_2, u_3](r - r^*) \\
&= \int_0^T \int_\Omega cr^*(r - r^*) dx dt + \int_0^T \int_\Omega f_{1,r}(b^*, w^*, h^*, r^*)(r - r^*)u_1 dx dt \\
&+ \int_0^T \int_\Omega f_{2,r}(b^*, w^*, h^*, r^*)(r - r^*)u_2 dx dt + \int_0^T \int_\Omega f_{3,r}(b^*, w^*, h^*, r^*)(r - r^*)u_3 dx dt, \qquad (12)
\end{aligned}
$$

where $r \in U_{ad}$ and $f_{i,r}$ $(i = 1, 2, 3)$ is the derivative of f_i with respect to r. Since r is arbitrary, substituting the partial derivative $f_{i,r}$ into Eq. (12) gives rise to the following variational inequality:

$$
\int_0^T \int_\Omega (cr^* + u_1)(r - r^*) dx dt \ge 0. \qquad (13)
$$

Additionally, it can be obtained from the variational inequality (13) that

$$
r^* = \mathbb{P}_{[r_1, r_2]}\{-\frac{1}{c}u_1\}, \qquad (14)
$$

where $\mathbb{P}$ is the projection defined as:

$$
\mathbb{P}_{[r_1, r_2]}(r) = \max\{r_1, \min\{r, r_2\}\}. \qquad (15)
$$

The proof is completed.

3. Main results

3.1. Method

In prior to showing the main results in this paper, we present the method used in our numerical simulations as well as the setting of relevant parameters.

The optimal control problem given by Eqs. (2)–(3) involves the objective functional (2), the state system (3), and the adjoint system (5). In order to obtain the numerical solution to the optimal control problem, we derive the finite difference equations of system (3) by employing the forward difference quotient in the time direction and the second-order central

difference quotient in the space direction. The approximation of the function b at the point (x_i, y_j, t_n) is denoted by b_{ij}^n. Therefore, the discretization system of (3) is as follows:

$$\begin{cases} \dfrac{b_{ij}^{n+1}-b_{ij}^n}{\Delta t} = \dfrac{b_{i+1,j}^n - 2b_{ij}^n + b_{i-1,j}^n}{(\Delta x)^2} + \dfrac{b_{i,j+1}^n - 2b_{ij}^n + b_{i,j-1}^n}{(\Delta x)^2} + f_1(b_{ij}^n, w_{ij}^n, h_{ij}^n, r_{ij}^n), \\ \dfrac{w_{ij}^{n+1}-w_{ij}^n}{\Delta t} = \delta_w \left(\dfrac{w_{i+1,j}^n - 2w_{ij}^n + w_{i-1,j}^n}{(\Delta x)^2} + \dfrac{w_{i,j+1}^n - 2w_{ij}^n + w_{i,j-1}^n}{(\Delta x)^2} \right) + f_2(b_{ij}^n, w_{ij}^n, h_{ij}^n, r_{ij}^n), \\ \dfrac{h_{ij}^{n+1}-h_{ij}^n}{\Delta t} = \delta_h \left(\dfrac{h_{i+1,j}^n - 2h_{ij}^n + h_{i-1,j}^n}{(\Delta x)^2} + \dfrac{h_{i,j+1}^n - 2h_{ij}^n + h_{i,j-1}^n}{(\Delta x)^2} \right) + f_3(b_{ij}^n, w_{ij}^n, h_{ij}^n, r_{ij}^n). \end{cases} \tag{16}$$

Similarly, the adjoint Eq. (5) can be discretized by using backward Euler method in the time direction, giving

$$\begin{cases} -\dfrac{{u_1}_{ij}^{n+1}-{u_1}_{ij}^n}{\Delta t} = \dfrac{{u_1}_{i+1,j}^{n+1} - 2{u_1}_{ij}^{n+1} + {u_1}_{i-1,j}^{n+1}}{(\Delta x)^2} + \dfrac{{u_1}_{i,j+1}^{n+1} - 2{u_1}_{ij}^{n+1} + {u_1}_{i,j-1}^{n+1}}{(\Delta x)^2} + \\ \qquad g_1(b_{ij}^{n+1}, w_{ij}^{n+1}, h_{ij}^n, r_{ij}^{n+1}, {u_1}_{ij}^{n+1}, {u_2}_{ij}^{n+1}, {u_3}_{ij}^{n+1}), \\ -\dfrac{{u_2}_{ij}^{n+1}-{u_2}_{ij}^n}{\Delta t} = \delta_w \left(\dfrac{{u_2}_{i+1,j}^{n+1} - 2{u_2}_{ij}^{n+1} + {u_2}_{i-1,j}^{n+1}}{(\Delta x)^2} + \dfrac{{u_2}_{i,j+1}^{n+1} - 2{u_2}_{ij}^{n+1} + {u_2}_{i,j-1}^{n+1}}{(\Delta x)^2} \right) + \\ \qquad g_2(b_{ij}^{n+1}, w_{ij}^{n+1}, h_{ij}^{n+1}, r_{ij}^{n+1}, {u_1}_{ij}^{n+1}, {u_2}_{ij}^{n+1}, {u_3}_{ij}^{n+1}), \\ -\dfrac{{u_3}_{ij}^{n+1}-{u_3}_{ij}^n}{\Delta t} = \delta_h \left(\dfrac{{u_3}_{i+1,j}^{n+1} - 2{u_3}_{ij}^{n+1} + {u_3}_{i-1,j}^{n+1}}{(\Delta x)^2} + \dfrac{{u_3}_{i,j+1}^{n+1} - 2{u_3}_{ij}^{n+1} + {u_3}_{i,j-1}^{n+1}}{(\Delta x)^2} \right) + \\ \qquad g_3(b_{ij}^{n+1}, w_{ij}^{n+1}, h_{ij}^{n+1}, r_{ij}^{n+1}, {u_1}_{ij}^{n+1}, {u_2}_{ij}^{n+1}, {u_3}_{ij}^{n+1}), \end{cases} \tag{17}$$

where $g_1 = f_{1,b}u_1 + f_{2,b}u_2 + f_{3,b}u_3$, $g_2 = f_{1,w}u_1 + f_{2,w}u_2 + f_{3,w}u_3$, $g_2 = f_{1,h}u_1 + f_{2,h}u_2 + f_{3,h}u_3$. And the discretized system for the objective functional $O[b, w, h, r]$ (2) can be written as:

$$\hat{O} = \frac{1}{2}\sum_{i,j=0}^{N}[a_1(b_{ij}^M - b_{ij}^{tar})^2 + a_2(w_{ij}^M - w_{ij}^{tar})^2 + a_3(h_{ij}^M - h_{ij}^{tar})^2] + \frac{\Delta t}{2}\sum_{i,j=0}^{N}\sum_{n=0}^{M-1}(cr_{ij}^n)^2. \tag{18}$$

Finally, we discretize the gradient of the objective function in the direction $r - r^*$ defined by variational inequalities (6)

$$\nabla_r O^n = cr^n + {u_1}^n. \tag{19}$$

The meanings and values of some of the parameters involved in the discrete process are as follows: $M = T/\Delta t$ is the total number of time steps, T is the time scale, Δt is the time step, $N = X/\Delta x + 1$ is the number of spatial nodes in a single direction, X is the spatial scale in a single direction, and Δx is the spatial step size. In our numerical experiments, these values are set to $T = 1$, $\Delta t = 0.001$, $X = 300$, and $\Delta x = 3$. In addition, we assume the Neumann boundary condition as well as the initial condition featuring random disturbance around the equilibrium point E_1^* ($E_1^{*'}$) or E_2^* ($E_2^{*'}$).

The goal in the optimal control problem is to find the minimum objective function (2). For such complex nonlinear problems, we apply the widespread gradient projection method (for details, see Ref. [45]). A schematic illustration of the algorithm for implementing the gradient projection approach is presented in Table 2. To get good agreement between the control pattern b_x^T and the target pattern b_x^{tar}, we choose $a_1 = a_2 = a_3 = 1$, and $c \ll 1$ (e.g., $c = 10^{-10}$). The target pattern b_x^{tar}, w_x^{tar} and h_x^{tar} is generated from the numerical results of the state Eq. (3).

3.2. Vegetation patterns with homogeneous human activities

In the case of homogeneous human activities, we treat the parameter r as a constant and investigate the impact of positive human activities ($r > 0$) and negative human activities ($r < 0$) on the structure of vegetation patterns, respectively.

Fig. 2 displays the structure of vegetation patterns for varying levels of positive human activities under different initial conditions. For the initial condition of random perturbations at equilibrium point E_2^*, stationary patterns of vegetation distribution can be observed (see Fig. 2(a_1)-(c_1)); in contrast, transient patterns are found if the initial condition is set by random perturbations at the equilibrium point E_1^* (see Fig. 2(a_2)-(c_2)). Moreover, it is shown from Fig. 2 that for either of the two initial conditions, the increase of positive human activities intensity does not lead to a phase transition in the vegetation pattern. This implies that positive human activities can maintain the pattern structure of vegetation.

Given the continuing presence of certain human activities that do harm to the vegetation growth, it is of great significance to investigate how negative human activities affect vegetation patterns. Fig. 3 shows the structure of vegetation patterns under the influence of negative human activities with different initial conditions. When the initial condition is chosen as random perturbations around $E_2^{*'}$ we obtain stationary patterns as demonstrated in Fig. 3(a_1)-(c_1).

Table 2
Algorithm for the gradient projection method.

Step: Process	
1:	**initialization**
2:	Select initial guess for r_0, initial step size $\lambda = 1$, $relErrorTol = 5.0e-2$, $k := 0$. Solve the state variables (b^0, w^0, h^0) in system (3), adjoint variables (u_1^0, u_2^0, u_3^0) in system (5). Calculate the relative error b^0 and b_T: $relError^0 = \frac{\|b^{0T}_x - b^{tar}_x\|_{L^2(\Omega)}}{\|b^{tar}_x\|_{L^2(\Omega)}}$.
3:	Set $maxcycle = 5000$.
4:	**end initialization**
5:	**main cycle**
6:	**while** $relError^k > relErrorTol \,\&\&\, k < maxcycle$ **do**
7:	$oldr \leftarrow r^k$, $old\nabla_r O \leftarrow \nabla_r O^k$;
8:	$k \leftarrow k + 1$;
9:	update control: $r^k = \mathbb{P}_{[r_1, r_2]}(r^{k-1} - \lambda \nabla_r O^{k-1})$;
10:	update state variables (b^k, w^k, h^k) by Eq. (16);
11:	update adjoint variables (u_1^0, u_2^0, u_3^0) by Eq. (17);
12:	update objective functional $\hat{O}^k$ by Eq. (18);
13:	update $\nabla_r O^k$ by Eq. (19); update $relError^k$;
14:	**if** $\|\hat{O}^k - \hat{O}^{k-1}\| < 10^{-10}$ **or** $\|relError^k - relError^{k-1}\| < 10^{-10}$ **or** $\lambda < 10^{-5}$ **do**
15:	**break**;
16:	**end if**
17:	**if** $\hat{O}^k > \hat{O}^{k-1}$ **do**
18:	$k \leftarrow k - 1$;
19:	$\lambda \leftarrow \lambda/2$;
20:	$r^k \leftarrow oldr$;
21:	$\nabla_r O^k \leftarrow old\nabla_r O$;
22:	**end if**
23:	**end while**
24:	**end main cycle**

However, when the initial condition is chosen as random perturbations around $E_1^{*'}$ we discover transient patterns as illustrated in Fig. 3(a_2)-(c_2). Besides, it is shown from Fig. 3 that as the strength of negative human activities increases (i.e., with the parameter value changing from $r = -0.005$ to $r = -0.01$ and to $r = -0.0134$), the structure of vegetation patterns evolves gradually from stripe to spot, and the gap between vegetation increases.

Fig. 4 showcases the changes of the average and maximum biomass of vegetation patterns caused by human activities. In the case of positive human activities (such as afforestation), the average biomass of vegetation in the steady state is proportional to the intensity of human activities, but the maximum density of vegetation displays a downward trend, indicating that the spatial distribution of vegetation is rather uniform. Conversely, in the case of negative human activities (such as logging and grazing), the vegetation biomass decreases with the intensity of negative human activities. Negative human activities will lead to the increase of vegetation isolation. Furthermore, it is found from Fig. 4 that in both cases of positive and negative human activities, the final average vegetation density of the pattern structure generated by the initial random perturbations near the equilibrium point E_1^* (or $E_1^{*'}$) is always lower than that generated by the initial random perturbations near the equilibrium point E_2^* (or $E_2^{*'}$).

3.3. Vegetation patterns with heterogeneous human activities

In the case of heterogeneous human activities, we treat the parameter r as a variable depending on both time and space, namely, $r = r_x^t$.

The effects of heterogeneity of human activities on vegetation patterns are exhibited in Fig. 5, where the structure of vegetation patterns is presented for different rainfalls. As shown in the first row of Fig. 5, in the absence of human activities (i.e., uncontrolled), the structure of vegetation patterns changes from the spot–stripe mixed pattern to the gap pattern, then to the hole pattern, and to the uniform state, correspondingly, as the value of the rainfall intensity p increases from 1.8375 to 2, then to 2.1, and to 2.2. The first column in Fig. 5 corresponds to the given target patterns, including the spot pattern (top), the labyrinth pattern (middle) and the gap pattern (bottom). It follows from Fig. 5 that when human activities are heterogeneously distributed in space, different original pattern structures for different rainfalls (as shown in the first row in Fig. 5) eventually evolve into the given target pattern structure. In particular, under appropriate intensities

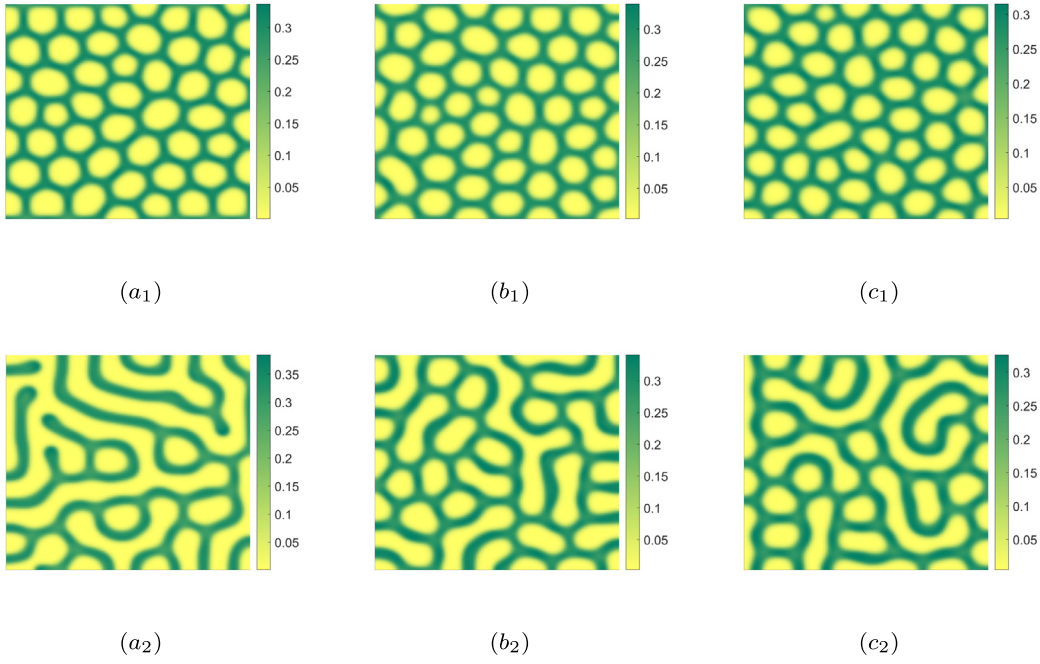

Fig. 2. The structure of vegetation patterns for positive human activities under different initial conditions. For the results in the first row (stationary patterns) the initial condition is set by random perturbations at the equilibrium point E_2^*, whereas for the results in second row (transient patterns) the initial condition is assumed with random fluctuations at the equilibrium point E_1^*. The value of human activities parameter is set to $r = 0.0002$ for (a_1) and (a_2), $r = 0.0012$ for (b_1) and (b_2), and $r = 0.0022$ for (c_1) and (c_2), respectively. The remaining parameters are the same as in Table 1.

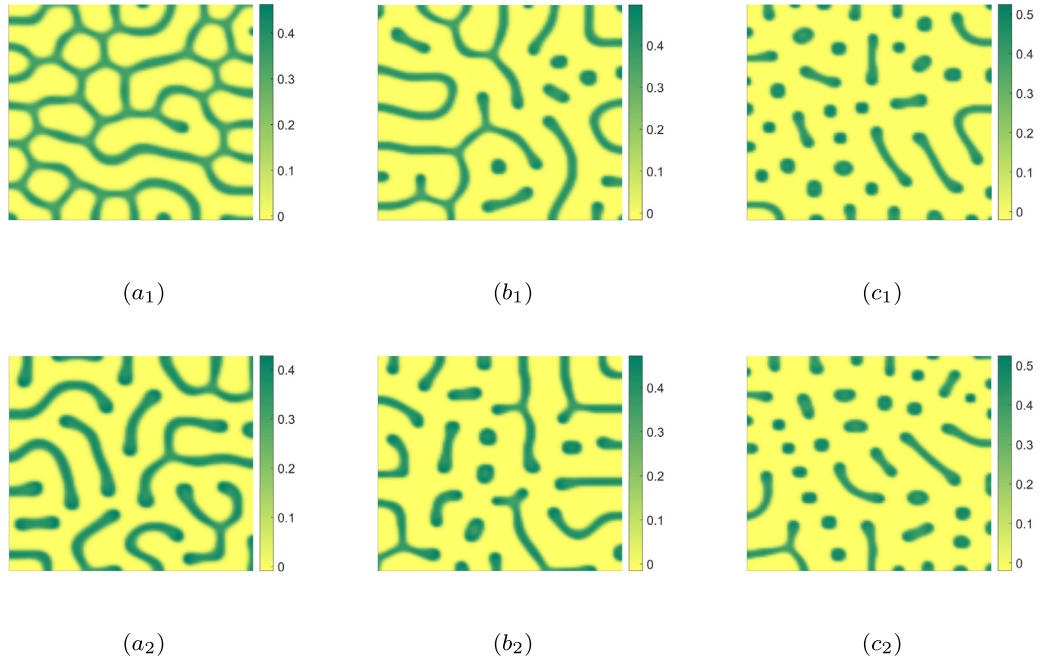

Fig. 3. The structure of vegetation patterns for negative human activities under different initial conditions. In panels (a_1)-(c_1), stationary patterns appear for the initial condition of random perturbations around $E_2^{*'}$, while in panels (a_2)-(c_2), transient patterns emerge for the initial condition of random perturbations around $E_1^{*'}$. The value of negative human activities is set to $r = -0.005$ for (a_1) and (a_2), $r = -0.01$ for (b_1) and (b_2), and $r = -0.0134$ for (c_1) and (c_2), respectively. The remaining parameters are the same as in Table 1.

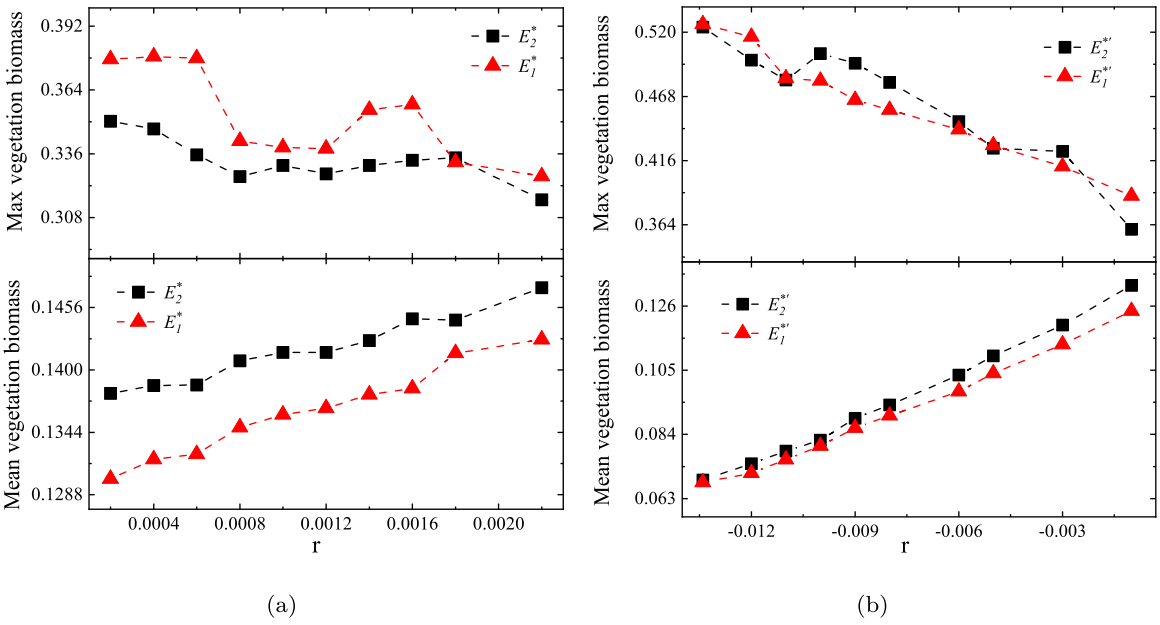

Fig. 4. Schematic diagram of the average and maximum biomass of vegetation at the steady state for different levels of human activities intensity: (a) $r > 0$, corresponding to positive human activities; (b) $r < 0$, standing for negative human activities. The black squares and red triangles represent initial conditions of random disturbances near equilibrium points E_2^* (or $E_2^{*'}$) and E_1^* (or $E_1^{*'}$), respectively.

of heterogeneous human activities, the vegetation pattern can evolve from the spot–stripe mixed pattern, the gap pattern, the hole pattern and the uniform state to given target patterns (see the second, fourth and sixth rows of Fig. 5). Moreover, the spatiotemporal heterogeneity of human activities can lead to the emergence of a regular pattern structure (see the last column of Fig. 5). Therefore, given the robustness (or vulnerability) of a certain kind of vegetation pattern structure, we can control the system to converge to or evolve away from such a pattern structure through appropriate human activities, thereby preventing the vegetation from desertification. In other words, our results can be well combined with the robustness of the ecosystem to provide guidance and suggestions for ecological protection. Furthermore, we show the distribution of human activities intensity and vegetation with iteration times under different initial states, taking the transition to the labyrinth pattern as an example. The simulation results show that the different initial states have no significant effect on the pattern transition (Fig. 6 and Fig. 7).

Fig. 8 reports the spatiotemporal average of human activities for different rainfalls when the vegetation pattern reaches such given target patterns as the spot, labyrinth, and gap patterns. In particular, it is found from Fig. 8 that the average intensity of human activities required for the vegetation to evolve to the spot pattern is higher than the one that is required for the vegetation to reach the labyrinth pattern, which in return is higher than that required to generate the gap pattern. Moreover, it is revealed that a higher rainfall implies a larger average intensity of human activities is needed for the vegetation to reach a fixed target pattern.

In order to better demonstrate that the desired pattern structure can be obtained through the influence of the heterogeneity of human activities, we use the relative error *relError* and the target functional value $O[b^*, w^*, h^*, r^*]$ to characterize the robustness of the result, with the relative error expressed as follows:

$$relError = \frac{\|b_x^T - b_x^{tar}\|_{L^2(\Omega)}}{\|b_x^{tar}\|_{L^2(\Omega)}}.$$

The variation of the relative error and target functional with the iteration count for different target patterns is showed in Fig. 9, from which we can see that the relative error approaches 0 as the iteration count increases, indicating that the results we obtain match nicely with the target pattern (see the first row in Fig. 9). From the evolution of the objective functional, we conclude that it is convergent as the iteration count increases. What is more, we can obtain the time (or cost) required for the system to evolve from the initial pattern to the target pattern (see the second row in Fig. 7). Compared with homogeneous human activities, heterogeneous human activities can enrich the dynamics of the system by inducing more complicated dynamical properties with wide potential applications. Typically, heterogeneous human activities can be readily managed with simple approaches to make the vegetation pattern transform to the desired state.

4. Conclusion and discussion

It can be argued that human activities have great impacts on vegetation dynamics. However, a systematic understanding of the impacts of the spatiotemporal heterogeneity of human activities on vegetation patterns is still lacking. In this

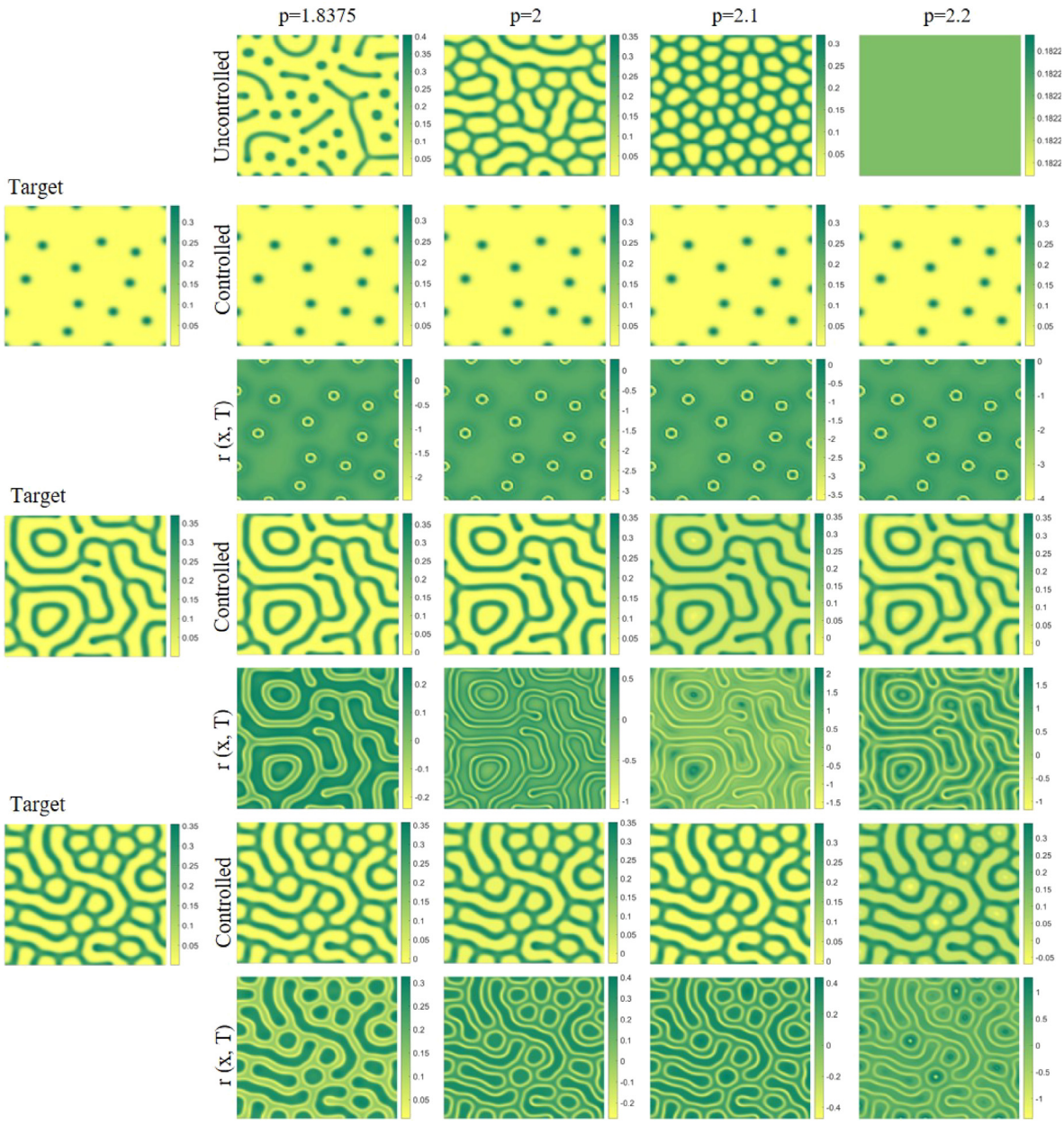

Fig. 5. Effects of spatial heterogeneity of human activities on vegetation pattern structures. The first row is the vegetation pattern structure under different rainfall intensity (which is marked by the parameter p) without the influence of human activities (uncontrolled). The first row presents three types of given target patterns including the spot pattern (top), the labyrinth pattern (middle) and the gap pattern (bottom). The third, fifth and seventh rows represent the spatial distribution of human activities r_x^T for generating the given target pattern. The remaining part corresponds to the corresponding vegetation pattern structure for different rainfalls when human activities are considered (controlled). The related parameters are as follows: $a_1 = a_2 = a_3 = 1$, and $c = 10^{-10}$. Other parameters are the same as in Table 1.

paper we address this issue by studying the dryland vegetation-water model via the aid of optimal control theory. To gain a good comparison and to underscore the effects of heterogeneity in human activities on vegetation dynamics, we split our study into two steps.

In the first step, the effects of positive and negative human activities on vegetation patterns are investigated in the case when the human activities are constant. The results show that increasing the intensity of positive human activities (such as afforestation) does not lead to the transformation between different types of vegetation pattern, but it will increase the average biomass of vegetation, which is beneficial to the growth of vegetation. Conversely, increasing the intensity of negative human activities (such as grazing and logging) will induce the gradual transformation from the stripe pattern to

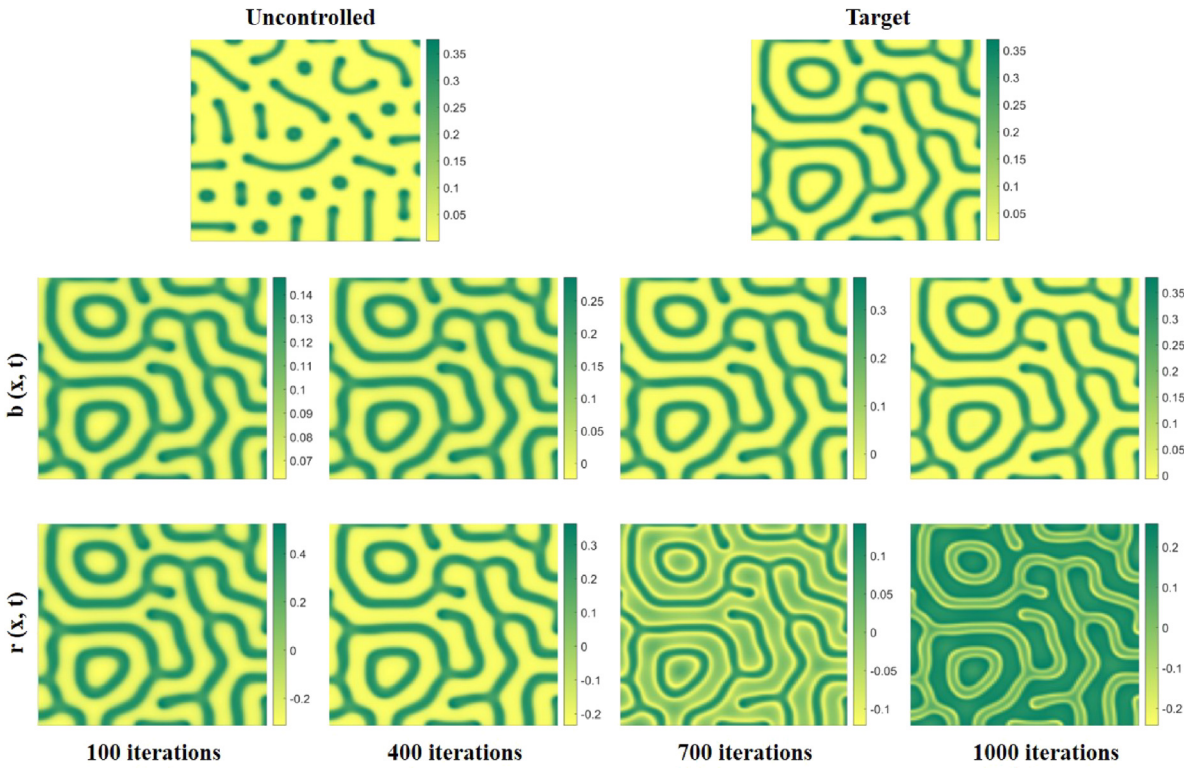

Fig. 6. The impact of spatial heterogeneity of human activities on the vegetation pattern structure at different iteration times. Without the influence of human activities heterogeneity, vegetation exhibits a mixed spatial distribution of spots and stripes (uncontrolled). Under the influence of spatiotemporal heterogeneity of human activities, vegetation gradually transforms into a labyrinth distribution (target). The initial state are $b_0 = b^* + 10^{-4}randn$ in Ω, $w_0 = w^* + 10^{-4}randn$ in Ω, $h_0 = h^* + 10^{-4}randn$ in Ω, where $randn$ is a random number with a standard normal distribution. The related parameters are as follows: $p = 1.8375$, $a_1 = a_2 = a_3 = 1$, and $c = 10^{-10}$. Other parameters are the same as in Table 1.

the spot pattern, and decrease the average biomass of vegetation. Additionally, it is found that the structure of vegetation patterns (either transient or stationary) depends on the initial condition (see Figs. 2 and 3).

In the second step, the effects of spatiotemporal heterogeneity of human activities on vegetation patterns are studied by the method of optimal control. Firstly, we establish the necessary conditions for the existence of the solution to the optimal control problem. Secondly, we uncover that the heterogeneity of human activities will enrich the vegetation dynamics by inducing phase transitions between different vegetation patterns, especially the transitions from the spot-strip mixed pattern, the gap pattern, the hole pattern and the uniform state to the given target pattern. Besides, we find that under appropriate human activities, each type of desired pattern structures can be obtained, implying the heterogeneity of human activities increases the diversity of pattern structure. Moreover, vegetation patterns generated in the case of high rainfalls for homogeneous circumstances can be obtained even in the case of low rainfalls for heterogeneous circumstances (see Figs. 5). Therefore, the heterogeneity of human activities facilitates the vegetation growth in low-rainfall regions, thereby reducing the desertification of vegetation. Furthermore, it is revealed that a regular vegetation pattern can emerge from a heterogeneous distribution of human activities with appropriate intensities.

It is well known that even simple spatial inhomogeneities can lead to spatiotemporal effects in reaction–diffusion systems, so the study of spatiotemporal heterogeneity has received much attention. For example, Benson et al. [28] conducted a very detailed branching analysis of reaction–diffusion systems with diffusion coefficients $D(x) = D + \eta x^2$ in the limit of $\eta \to 0$, showing that small heterogeneity can yield rich dynamical properties. Some scholars have shown that the heterogeneity contained in pattern formation systems can induce spatiotemporal oscillations [29]. In contrast to previous work on heterogeneity, this paper combines optimal control theory with a dryland vegetation water model to reveal the impact of spatio-temporal heterogeneity in human activities on vegetation pattern structures. It is shown that spatio-temporal heterogeneity of human activities can induce rich pattern structures. In summary, this paper presents a general framework for studying the effects of spatiotemporal heterogeneity from the perspective of optimal control.

The results of this paper provide new insights for ecological management of dryland as well as biodiversity conservation. As is known to all, a poor rainfall is a typical feature of dryland, and the rainfall is the key element for vegetation growth. Obviously, it is difficult to promote vegetation growth by improving such natural conditions as the rainfall and sunlight. Our results show that under the influence of the spatiotemporal heterogeneity in human activities, the pattern

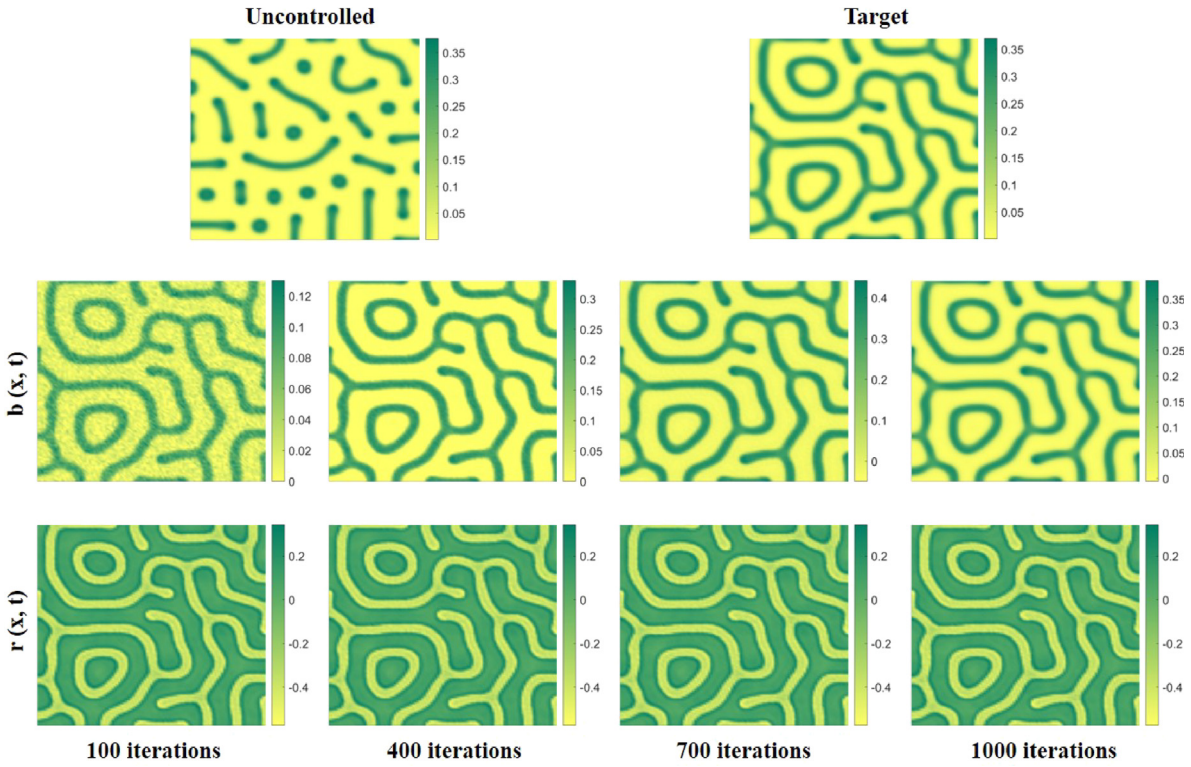

Fig. 7. The impact of spatial heterogeneity of human activities on the vegetation pattern structures at different iteration times. The initial state are $b_0 = b^* + 10^{-2} randn$ in Ω, $w_0 = w^* + 10^{-2} randn$ in Ω, $h_0 = h^* + 10^{-2} randn$ in Ω.

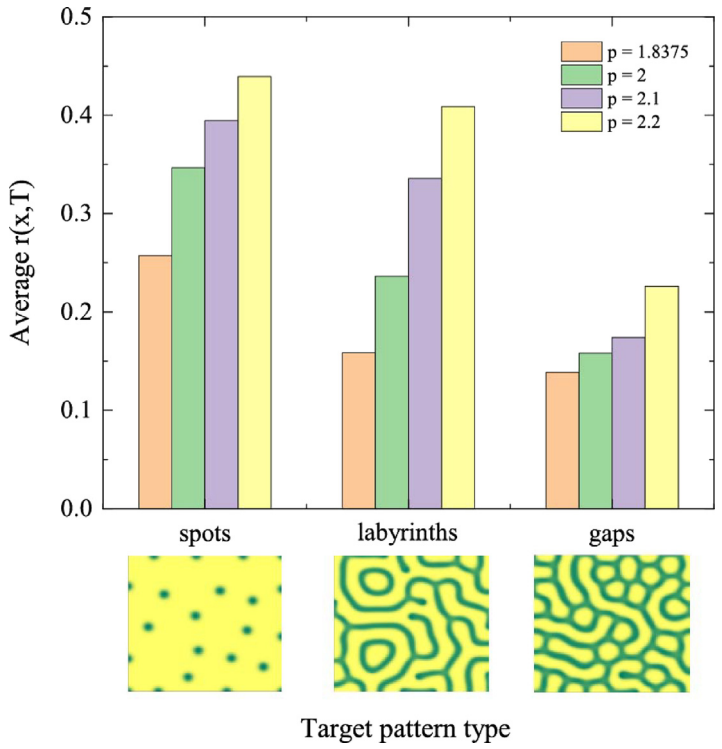

Fig. 8. The spatiotemporal average intensity of human activities required for the vegetation to reach the target patterns for different rainfalls. The required intensity of human activities is directly proportional to the rainfall when the target pattern remains constant. The average human activities required for the three types (i.e., spot, labyrinth and gap) of target patterns to be generated are sorted in the order of Spot>Labyrinth>Gap.

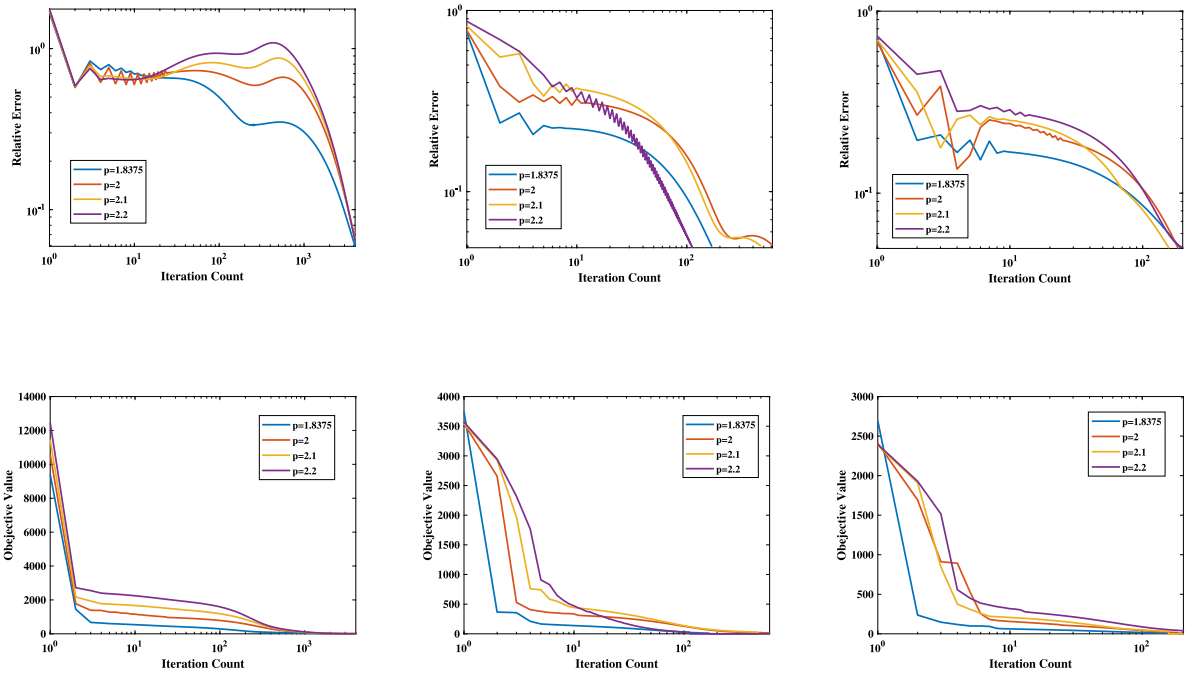

Fig. 9. The variation of relative error and objective function with the iteration count k for different target patterns. The first row is the relative error with $\frac{\|b_x^{kT}-b_x^{tar}\|_{L^2(\Omega)}}{\|b_x^{tar}\|_{L^2(\Omega)}}$ and the second row is the objection functional $O^k[b^*, w^*, h^*, r^*]$. (a)(d) The target pattern is a spot pattern; (b)(e) The target pattern is a labyrinth pattern; (c)(f) The target pattern is a gap pattern.

structure can change even if the rainfall is very low. Therefore, it is feasible to improve vegetation growth by regulating human activities. Existing studies have shown that the spot pattern is an early warning signal of desertification [13]. In this sense, we can adopt strategies to control the vegetation to evolve to other pattern structures, thus effectively avoid the occurrence of desertification. Meanwhile, Bertolini et al. shows that the labyrinth pattern is a relatively stable pattern structure [46]. For such a reason, we can provide suggestions for administrating human activities to induce the vegetation to evolve to this pattern structure, and then improve the stability of vegetation systems.

CRediT authorship contribution statement

Li-Feng Hou: Writing – original draft, Methodology, Software. **Gui-Quan Sun:** Conceptualization, Writing – review & editing. **Matjaž Perc:** Writing – review & editing.

Declaration of competing interest

The authors declare that they have no known competing financial interests or personal relationships that could have appeared to influence the work reported in this paper.

Data availability

No data was used for the research described in the article

Acknowledgments

This work is supported by the National Key Research and Development Program of China (Grant No. 2018YFE0109600), National Natural Science Foundation of China under Grant Nos. 42075029 and 42275034.

Appendix. Elements of Jacobian matrix of system (1) without spatial effects

$$
\begin{aligned}
a_{11} =& 2w^*b^*(1-b^*)(1+\eta b^*) - w^*(b^*-1)(b^*\eta+1)^2 - w^*b^*(1+\eta b^*)^2 - 1,\\
a_{12} =& -(b^*-1)(1+\eta b^*)^2 b^*,\\
a_{21} =& \frac{\alpha h^*}{q+b^*} - \frac{\alpha h^*(qf+b^*)}{(q+b^*)^2} + \frac{\nu_w R_w w^*}{(1+R_w b^*)^2} - \gamma w^*(b^*\eta+1)^2 - 2b^*\gamma\eta w^*(b^*\eta+1),\\
a_{22} =& -\frac{\nu_w}{1+R_w b^*} - \gamma b^*(1+\eta b^*)^2 < 0,\\
a_{23} =& \frac{\alpha(qf+b^*)}{q+b^*} > 0,\\
a_{31} =& -\frac{\alpha h^*}{q+b^*} + \frac{\alpha h^*(qf+b^*)}{(q+b^*)^2} + \frac{\nu_h R_h h^*}{(1+R_h b^*)^2},\\
a_{33} =& -\frac{\alpha(qf+b^*)}{q+b^*} - \frac{\nu_h}{1+R_h b^*} < 0.
\end{aligned}
$$

References

[1] Mohammad AG, Adam MA. The impact of vegetative cover type on runoff and soil erosion under different land uses. Catena 2010;81:97–103. http://dx.doi.org/10.1016/j.catena.2010.01.008.
[2] Lemordant L, Gentine P, Swann AS, Cook BI, Scheff J. Critical impact of vegetation physiology on the continental hydrologic cycle in response to increasing CO_2. Proc Natl Acad Sci USA 2018;115:4093–8. http://dx.doi.org/10.1073/pnas.1720712115.
[3] Liu S, Huang S, Xie Y, Wang H, Huang Q, Leng G, et al. Spatial-temporal changes in vegetation cover in a typical semi-humid and semi-arid region in China: Changing patterns, causes and implications. Ecol Indic 2019;98:462–75. http://dx.doi.org/10.1016/j.ecolind.2018.11.037.
[4] Sun G-Q, Wang C-H, Chang L-L, Wu Y-P, Li L, Jin Z. Effects of feedback regulation on vegetation patterns in semi-arid environments. Appl Math Model 2018;61:200–15. http://dx.doi.org/10.1016/j.apm.2018.04.010.
[5] Gilad E, von Hardenberg J, Provenzale A, Shachak M, Meron E. A mathematical model of plants as ecosystem engineers. J Theoret Biol 2007;244:680–91. http://dx.doi.org/10.1016/j.jtbi.2006.08.006.
[6] Klausmeier CA. Regular and irregular patterns in semiarid vegetation. Science 1999;284:1826–8. http://dx.doi.org/10.1126/science.284.5421.1826.
[7] Rietkerk M, Boerlijst MC, van Langevelde F, HilleRisLambers R, de Koppel Jv, Kumar L, et al. Self-organization of vegetation in arid ecosystems. Amer Nat 2002;160:524–30. http://dx.doi.org/10.1086/342078.
[8] Rietkerk M, Dekker SC, De Ruiter PC, van de Koppel J. Self-organized patchiness and catastrophic shifts in ecosystems. Science 2004;305:1926–9. http://dx.doi.org/10.1126/science.1101867.
[9] Eigentler L, Sherratt JA. Effects of precipitation intermittency on vegetation patterns in semi-arid landscapes. Physica D 2020;405:132396. http://dx.doi.org/10.1016/j.physd.2020.132396.
[10] Lefever R, Lejeune O. On the origin of tiger bush. Bull Math Biol 1997;59:263–94. http://dx.doi.org/10.1007/BF02462004.
[11] Lejeune O, Tlidi M. A model for the explanation of vegetation stripes (tiger bush). J Veg Sci 1999;10:201–8. http://dx.doi.org/10.2307/3237141.
[12] Lejeune O, Tlidi M, Couteron P. Localized vegetation patches: a self-organized response to resource scarcity. Phys Rev E 2002;66:010901. http://dx.doi.org/10.1103/PhysRevE.66.010901.
[13] von Hardenberg J, Meron E, Shachak M, Zarmi Y. Diversity of vegetation patterns and desertification. Phys Rev Lett 2001;87:198101. http://dx.doi.org/10.1103/PhysRevLett.87.198101.
[14] Meron E, Gilad E, Von Hardenberg J, Shachak M, Zarmi Y. Vegetation patterns along a rainfall gradient. Chaos Solitons Fractals 2004;19:367–76. http://dx.doi.org/10.1016/S0960-0779(03)00049-3.
[15] Zelnik YR, Meron E, Bel G. Gradual regime shifts in fairy circles. Proc Natl Acad Sci USA 2015;112:12327–31. http://dx.doi.org/10.1073/pnas.1504289112.
[16] Gilad E, von Hardenberg J, Provenzale A, Shachak M, Meron E. Ecosystem engineers: from pattern formation to habitat creation. Phys Rev Lett 2004;93:098105. http://dx.doi.org/10.1103/PhysRevLett.93.098105.
[17] HilleRisLambers R, Rietkerk M, van den Bosch F, Prins HH, de Kroon H. Vegetation formation in semi-arid grazing systems. Ecology 2001;82:50–61. http://dx.doi.org/10.1890/0012-9658(2001)082.
[18] Sun G-Q, Zhang H-T, Song Y-L, Li L, Jin Z. Dynamic analysis of a plant-water model with spatial diffusion. J Differential Equations 2022;329:395–430. http://dx.doi.org/10.1016/j.jde.2022.05.009.
[19] Meron E. Pattern formation–a missing link in the study of ecosystem response to environmental changes. Math Biosci 2016;271:1–18. http://dx.doi.org/10.1016/j.mbs.2015.10.015.
[20] Wang J, Wang K, Zhang M, Zhang C. Impacts of climate change and human activities on vegetation cover in hilly southern China. Ecol Eng 2015;81:451–61. http://dx.doi.org/10.1016/j.ecoleng.2015.04.022.
[21] Huang S, Zheng X, Ma L, Wang H, Huang Q, Leng G, et al. Quantitative contribution of climate change and human activities to vegetation cover variations based on GA-SVM model. J Hydrol 2020;584:124687. http://dx.doi.org/10.1016/j.jhydrol.2020.124687.
[22] Sun G-Q, Zhang H-T, Wang J-S, Li J, Wang Y, Li L, et al. Mathematical modeling and mechanisms of pattern formation in ecological systems: a review. Nonlinear Dynam 2021;104:1677–96. http://dx.doi.org/10.1007/s11071-021-06314-5.
[23] Mahmoud SH, Gan TY. Impact of anthropogenic climate change and human activities on environment and ecosystem services in arid regions. Sci Total Environ 2018;633:1329–44. http://dx.doi.org/10.1016/j.scitotenv.2018.03.290.
[24] Cai D, Ge Q, Wang X, Liu B, Goudie AS, Hu S. Contributions of ecological programs to vegetation restoration in arid and semiarid China. Environ Res Lett 2020;15:114046. http://dx.doi.org/10.1088/1748-9326/abbde9.
[25] Cao S, Chen L, Shankman D, Wang C, Wang X, Zhang H. Excessive reliance on afforestation in China's arid and semi-arid regions: lessons in ecological restoration. Earth-Sci Rev 2011;104:240–5. http://dx.doi.org/10.1016/j.earscirev.2010.11.002.
[26] Ge Z, Liu Q-X. Foraging behaviours lead to spatiotemporal self-similar dynamics in grazing ecosystems. Ecol Lett 2022;25:378–90. http://dx.doi.org/10.1111/ele.13928.
[27] Jiang L, Bao A, Guo H, Ndayisaba F, et al. Vegetation dynamics and responses to climate change and human activities in Central Asia. Sci Total Environ 2017;599:967–80. http://dx.doi.org/10.1016/j.scitotenv.2017.05.012.

[28] Benson DL, Maini PK, Sherratt JA. Unravelling the Turing bifurcation using spatially varying diffusion coefficients. J Math Biol 1998;37:381–417. http://dx.doi.org/10.1007/s002850050135.
[29] Krause AL, Klika V, Woolley TE, Gaffney EA. Heterogeneity induces spatiotemporal oscillations in reaction-diffusion systems. Phys Rev E 2018;97:052206. http://dx.doi.org/10.1103/PhysRevE.97.052206.
[30] Gandhi P, Werner L, Iams S, Gowda K, Silber M. A topographic mechanism for arcing of dryland vegetation bands. J R Soc Interface 2018;15:20180508. http://dx.doi.org/10.1098/rsif.2018.0508.
[31] Bastiaansen R, Dijkstra HA, von der Heydt AS. Fragmented tipping in a spatially heterogeneous world. Environ Res Lett 2022;17:045006. http://dx.doi.org/10.1088/1748-9326/ac59a8.
[32] Asamoah JKK, Okyere E, Abidemi A, Moore SE, Sun G-Q, Jin Z, et al. Optimal control and comprehensive cost-effectiveness analysis for COVID-19. Results Phys 2022;33:105177. http://dx.doi.org/10.1016/j.rinp.2022.105177.
[33] Asamoah JKK, Yankson E, Okyere E, Sun G-Q, Jin Z, Jan R, et al. Optimal control and cost-effectiveness analysis for dengue fever model with asymptomatic and partial immune individuals. Results Phys 2021;31:104919. http://dx.doi.org/10.1016/j.rinp.2021.104919.
[34] Chang L, Gao S, Wang Z. Optimal control of pattern formations for an SIR reaction–diffusion epidemic model. J Theoret Biol 2022;536:111003. http://dx.doi.org/10.1016/j.jtbi.2022.111003.
[35] Liu C, Gao S, Song M, Bai Y, Chang L, Wang Z. Optimal control of the reaction–diffusion process on directed networks. Chaos 2022;32:063115. http://dx.doi.org/10.1063/5.0087855.
[36] Gao S, Chang L, Romić I, Wang Z, Jusup M, Holme P. Optimal control of networked reaction–diffusion systems. J R Soc Interface 2022;19:20210739. http://dx.doi.org/10.1098/rsif.2021.0739.
[37] Getzin S, Yizhaq H, Bell B, Erickson TE, Postle AC, Katra I, et al. Discovery of fairy circles in Australia supports self-organization theory. Proc Natl Acad Sci USA 2016;113:3551–6. http://dx.doi.org/10.1073/pnas.1522130113.
[38] Murugavel K, Srithar K. Performance study on basin type double slope solar still with different wick materials and minimum mass of water. Renew Energy 2011;36:612–20. http://dx.doi.org/10.1016/j.renene.2010.08.009.
[39] Eigentler L, Sherratt JA. Metastability as a coexistence mechanism in a model for dryland vegetation patterns. Bull Math Biol 2019;81:2290–322. http://dx.doi.org/10.1007/s11538-019-00606-z.
[40] Majumdar S, Das Pan N. Combining opensource GIS and meta-analysis to link rainfall trend and human activity: case study on Gumti and Khowai drainage systems, Tripura, India. Spat Inf Res 2020;28:287–98. http://dx.doi.org/10.1007/s41324-019-00288-8.
[41] Trenberth KE. Climate change caused by human activities is happening and it already has major consequences. J Energy Nat Resour Law 2018;36:463–81. http://dx.doi.org/10.1080/02646811.2018.1450895.
[42] Garvie MR, Trenchea C. Optimal control of a nutrient-phytoplankton-zooplankton-fish system. SIAM J Control Optim 2007;46:775–91. http://dx.doi.org/10.1137/050645415.
[43] Garvie MR, Trenchea C. Identification of space-time distributed parameters in the Gierer–Meinhardt reaction-diffusion system. SIAM J Appl Math 2014;74:147–66. http://dx.doi.org/10.1137/120885784.
[44] Tröltzsch F. Optimal control of partial differential equations: theory, methods, and applications. Graduate studies in mathematics, vol. 112, American Mathematical Soc. 2010.
[45] De los Reyes JC. Numerical PDE-constrained optimization. Springer; 2015.
[46] Bertolini C, Cornelissen B, Capelle J, Van De Koppel J, Bouma TJ. Putting self-organization to the test: labyrinthine patterns as optimal solution for persistence. Oikos 2019;128:1805–15. http://dx.doi.org/10.1111/oik.06373.